AIP | Review of Scientific Instruments

# Simulation-guided optimization of small-angle analyzer geometry in the neutron backscattering spectrometer SPHERES

Joachim Wuttke and Michaela Zamponi

Citation: Review of Scientific Instruments **84**, 115108 (2013); doi: 10.1063/1.4831815
View online: http://dx.doi.org/10.1063/1.4831815
View Table of Contents: http://scitation.aip.org/content/aip/journal/rsi/84/11?ver=pdfcov
Published by the AIP Publishing

# Simulation-guided optimization of small-angle analyzer geometry in the neutron backscattering spectrometer SPHERES

Joachim Wuttke[a] and Michaela Zamponi
*Forschungszentrum Jülich GmbH, Jülich Centre for Neutron Science at MLZ, Lichtenbergstraße 1, 85747 Garching, Germany*

(Received 11 September 2013; accepted 3 November 2013; published online 21 November 2013)

The resolution of neutron backscattering spectrometers deteriorates at small scattering angles where analyzers deviate from exact backscattering. By reducing the azimuth angle range of the analyzers, the resolution can be improved with little loss of peak intensity. Measurements at the spectrometer SPHERES are in excellent agreement with simulations, which proves the dominance of geometric effects. © *2013 AIP Publishing LLC*. [http://dx.doi.org/10.1063/1.4831815]

## I. INTRODUCTION

In neutron backscattering spectrometers, spectra at small scattering angles $2\vartheta \lesssim 30^\circ$ are of comparatively poor quality, for no less than three different reasons: *First*, count rates are low because the solid angle covered by one detector is proportional to $\vartheta$. *Second*, the relative wavenumber spread $\Delta q/q$ is proportional to $\Delta\vartheta/\vartheta$ so that a scattering law $S(q, \omega)$ that varies with $q$ is more smeared the smaller $\vartheta$ is. *Third*, small-angle analyzers cannot be aligned to an exact backscattering geometry because detectors must be placed outside the incoming neutron beam. In contrast, large-angle analyzers focus neutrons exactly back onto the sample.

While we can do nothing about the first problem, and little about the second, the third merits a closer look. A small-angle analyzer ring is a segment of a sphere. To focus from the sample into a detector, the center of this sphere must be halfway between the sample and the detector (point + in Fig. 1). As a consequence, the analyzer Bragg reflection angle $2\Theta$ deviates from exact backscattering ($2\Theta = \pi$). Furthermore, the rotational symmetry around the direction of the incident beam is broken, which causes $2\Theta$ to vary around the ring, as exemplified in Fig. 1, where the section opposite the detector is much closer to exact backscattering than the rest of the ring. This spread of reflection angles leads to a broadening of the resolution function, which in some cases can even become twin-peaked.

In this paper, we present measurements and simulations that show how this geometry influences the resolution of the backscattering spectrometer SPHERES.[1] Guided by simulations, we covered part of the analyzer rings by cadmium plates. As expected, the resolution function became narrower and more regularly shaped with little loss of peak intensity. This is now the routine configuration of SPHERES.

## II. FUNDAMENTALS

### A. Backscattering scans

Backscattering instruments select neutron energies $E_{\mathrm{i,f}}$ to measure inelastic scattering spectra as a function of the sample energy gain $\Delta E := E_\mathrm{i} - E_\mathrm{f}$. In SPHERES, $E_\mathrm{f}$ is fixed at a nominal value $E_0 = 2.08$ meV, given by the backscattering condition for Si(111); $E_\mathrm{i}$ is swept over a dynamic range of $E_0 \pm 30$ $\mu$eV using the Doppler effect in the oscillating monochromator. While sample spectra are usually analyzed as a function of the energy transfer $\Delta E$, the instrument physics is better studied in terms of neutron wavenumbers $k$, with $E = \hbar^2k^2/2/m_n$. In the present study we are only concerned with resolution spectra that extend over no more than a few $\mu$eV so that we may linearize the dispersion relation as $E/E_0 \doteq 2k/k_0$, with $k_0 = 1.002$ Å$^{-1}$.

Each deviation $\chi := \pi/2 - \Theta$ from perfect backscattering means that the reflected wavenumber $k$ is larger than the ideal value $k_0$, according to the Bragg condition

$$k \cos\chi = k_0. \tag{1}$$

This can be expressed as a geometric wavenumber shift

$$\delta k^{\mathrm{geo}} := k_0 \left(\frac{1}{\cos\chi} - 1\right). \tag{2}$$

The leading order for small $\chi$ is quadratic:

$$\delta k^{\mathrm{geo}} \doteq k_0 \frac{\chi^2}{2}. \tag{3}$$

In addition, we have a randomly distributed resolution shift and a Doppler shift so that neutrons reach the sample with a wavenumber

$$k_\mathrm{i} = k_0 + \delta k_\mathrm{i}^{\mathrm{geo}} + \delta k_\mathrm{i}^{\mathrm{res}} + \delta k_\mathrm{i}^{\mathrm{Dop}}. \tag{4}$$

Scattered neutrons are reflected by the analyzer if

$$k_\mathrm{f} = k_0 + \delta k_\mathrm{f}^{\mathrm{geo}} + \delta k_\mathrm{f}^{\mathrm{res}}. \tag{5}$$

The data acquisition software of the spectrometer, of course, knows nothing about geometric and intrinsic resolution shifts. It increments histograms according to the nominal energy transfer given by the velocity of the Doppler drive,

$$\Delta E = \frac{2E_0}{k_0}(k_\mathrm{i}^{\mathrm{nom}} - k_\mathrm{f}^{\mathrm{nom}}) = \frac{2E_0}{k_0}\delta k_\mathrm{i}^{\mathrm{Dop}}. \tag{6}$$

Treating the test sample used in resolution measurements as an ideal elastic scatterer, we equate (4) and (5), and obtain a relation between the apparent wavenumber transfer and the

[a]Electronic mail: j.wuttke@fz-juelich.de

 

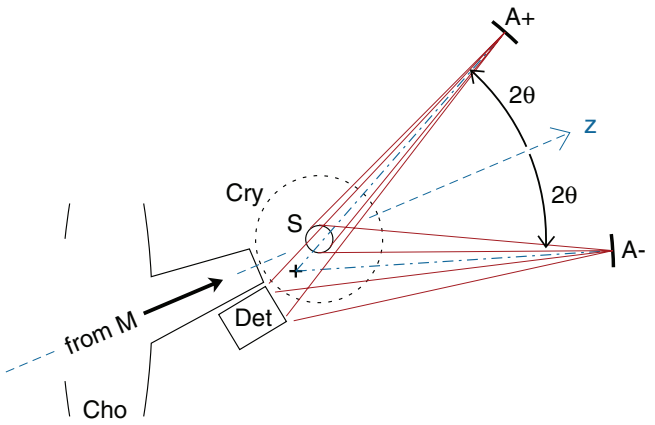


FIG. 1. Geometry of the secondary spectrometer of the backscattering instrument SPHERES.[1] Cho: chopper vacuum housing; From M: incident beam, from monochromator, defining the $z$ axis; S: sample; Det: detector; Cry: cryostat tail, imposing a minimum distance S–Det; A: horizontal section through a small-angle analyzer ring. This ring is part of a sphere that is centered at point +, halfway between S and Det. While the segment A+ is almost perfectly aligned to backscattering, the segment A− deviates so strongly from backscattering that it deteriorates the resolution.

actual resolution effects,

$$\delta k_{\mathrm{i}}^{\mathrm{Dop}} = \delta k_{\mathrm{f}}^{\mathrm{geo}} - \delta k_{\mathrm{i}}^{\mathrm{geo}} + \delta k_{\mathrm{f}}^{\mathrm{res}} - \delta k_{\mathrm{i}}^{\mathrm{res}}. \tag{7}$$

Equations (6) and (7) provide a recipe for computing a resolution profile from simulated neutron trajectories and from random draws of $\delta k_{\mathrm{i,f}}^{\mathrm{res}}$.

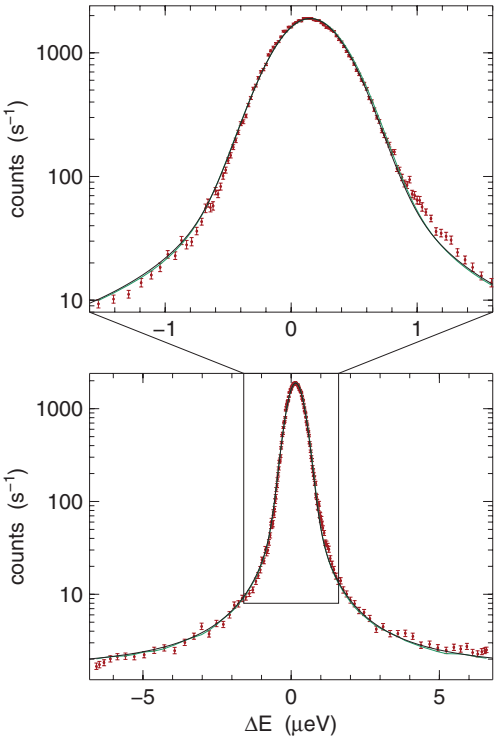


FIG. 2. Resolution of the regular large-angle detectors of SPHERES. Symbols: Elastic scattering by a typical frozen organic sample (cyclo-hexanol at 4 K in a standard hollow cylinder, outer diameter 25 mm, illuminated height about 45 mm) at $2\vartheta = 40 \pm 15^{\circ}$. Black line: fit with a flat background (1.54 s$^{-1}$) plus a Voigt profile ($\sigma = 0.244$ $\mu$eV, $\gamma = 0.052$ $\mu$eV, centered at 0.15 $\mu$eV). Green line, almost indistinguishable from the black line: Simulation with BASTSCHO as described in Sec. III B.

### B. Intrinsic resolution from large-angle spectra

For a complete spectrometer simulation, we must draw random shifts $\delta k_{\mathrm{i,f}}^{\mathrm{res}}$ from a distribution that describes the intrinsic reflection profile of the bent silicon crystals used in the monochromator and analyzer. We approximate this distribution by a simple mathematical model, the Voigt function $V(k;\sigma,\gamma)$. This is the convolution of a Gaussian with standard deviation $\sigma$ and a Lorentzian with width parameter $\gamma$ (half width at half maximum). The Gaussian dominates the center of the distribution, whereas the Lorentzian accounts for the Darwin wings of the perfect crystal reflectivity.

To use the Voigt function as input for our simulation, we need to fix its two parameters $\sigma$ and $\gamma$. Many measurements have firmly established that the resolution of SPHERES, under regular backscattering conditions at large scattering angles, varies little with sample geometry. Therefore, in a first approximation we can parametrize $V$ by fitting it to a measured resolution spectrum, ignoring all geometry effects. For the numeric computation of $V$, a recent reimplementation of the Faddeeva function is used.[2]

Figure 2 shows a resolution spectrum of SPHERES as measured in the two large-angle detectors with the best signal-to-noise ratio on a logarithmic intensity scale. Energy channels are flexibly rebinned to achieve relative errors smaller than 9%. The observed full width at half maximum (FWHM) of $1.45 \times 10^{-4} k_0$ agrees in magnitude with the expectations from a simple model of the bent crystals [Ref. 1, Sec. III C]. The figure includes a fit with a shifted Voigt function plus flat background; data bins are weighed in standard way by the reciprocal variance. The fit is not perfect, but quite sufficient for our present purpose. According to the fit, the signal-to-noise ratio is 1233:1; in normal operation (spectrometer housing filled with argon) it would be about 40% better.

The resolution spectrum is visibly displaced with respect to nominal elastic scattering at zero energy transfer. This displacement is regularly observed at SPHERES, and typically shows a weak but systematic dependence on the sample temperature. It is not understood at present. To account for it in the following simulations, a fixed offset of $3.1 \times 10^{-5} k_0$ is imposed *ad hoc*.

### C. Off-backscattering geometry

At large-scattering angles, with analyzers aligned to focus back onto the sample, deviations from perfect backscattering only arise from the finite cross section of the incoming beam, of the sample, and of the detectors. With a maximum rectangular sample section of $30 \times 40$ mm$^2$ and an analyzer radius of 2000 mm, the off-scattering angle $\chi$ is rarely larger than $10^{-3}$. With (3), the geometric wavenumber shift is smaller than $10^{-6} k_0$, and almost two orders of magnitudes below the Gaussian standard deviation of the intrinsic resolution function. Hence, geometric effects are negligible at large scattering angles.

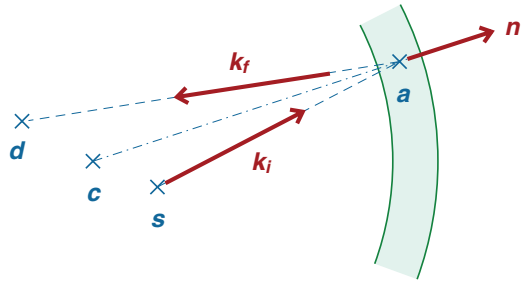


FIG. 3. Geometry of approximative backscattering by a spherical monochromator or analyzer centered at $\boldsymbol{c}$. The thickness of the crystal layer is enormously exaggerated.

At small scattering angles, each analyzer ring is a segment of a sphere of radius $R$. It acts as a concave mirror that maps the sample position $\boldsymbol{s}$ onto the detector position $\boldsymbol{d}$. To achieve this, the ring is centered at $\boldsymbol{c} = (\boldsymbol{s} + \boldsymbol{d})/2$, as shown in Fig. 3. Let $\boldsymbol{a}$ be a point on the ring. The surface normal at $\boldsymbol{a}$ points in the direction of $\boldsymbol{a} - \boldsymbol{c}$. Neutrons reach $\boldsymbol{a}$ if they have been scattered at $\boldsymbol{s}$ in the direction of $\boldsymbol{a} - \boldsymbol{s}$. They are then eligible for Bragg reflection with

$$\cos\chi = \frac{(\boldsymbol{a}-\boldsymbol{s})(\boldsymbol{a}-\boldsymbol{c})}{|\boldsymbol{a}-\boldsymbol{s}|\cdot|\boldsymbol{a}-\boldsymbol{c}|}. \tag{8}$$

Let us choose the origin at $\boldsymbol{s} := 0$. The relative geometric wavenumber shift (2) is then

$$\frac{\delta k}{k_0} = \frac{R|\boldsymbol{a}-\boldsymbol{c}|}{\boldsymbol{a}(\boldsymbol{a}-\boldsymbol{c})} - 1. \tag{9}$$

Assuming $c \ll R$ and expanding to the lowest nonvanishing order, we obtain

$$\frac{\delta k}{k_0} \doteq \frac{c^2}{2r^2}\,|\hat{\boldsymbol{a}} \times \hat{\boldsymbol{c}}|^2\,. \tag{10}$$

The cross product vanishes if $\boldsymbol{a}$ is collinear with the sample and the detector, as is the case for analyzer segment $A_+$ in Fig. 1.

In the unfavorable case $A_-$, the cross product in (10) has the maximum value

$$\max|\hat{\boldsymbol{a}} \times \hat{\boldsymbol{c}}| = \sin(\beta + 2\theta), \tag{11}$$

where the angle $\beta$ measures the deviation of $\boldsymbol{c} - \boldsymbol{s}$ from the optical axis. For the current detector arrangement of SPHERES, shown in Fig. 4, rings 5,6 at $2\theta = 19.5° \pm 2.9°$ deviate most from backscattering. The center of the detector entrance window is located at $\boldsymbol{d} = (60, 60, 95)$ mm, hence $\beta \simeq \arctan(85/95) \simeq 42°$, $\max|\hat{\boldsymbol{a}} \times \hat{\boldsymbol{c}}| \simeq 0.9$, $c \simeq 64$ mm. Comparing (10) with (3), we obtain a maximum off-backscattering angle $\chi$ of $8.3 \times 10^{-4}$. The corresponding geometric wavenumber shift of $\delta k \simeq 4.2 \times 10^{-4} k_0$ is considerably larger than the FWHM of the large-angle resolution function of $1.45 \times 10^{-4} k_0$. Geometric effects clearly dominate the resolution at off-backscattering detectors.

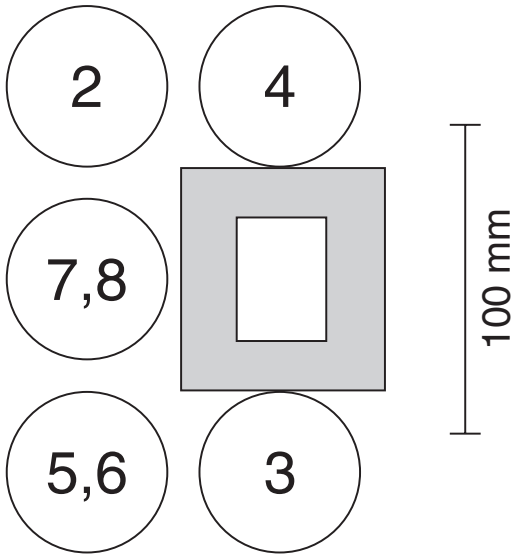


FIG. 4. Location of small-angle detectors as of May 2013. View from the analyzers towards the chopper. The rectangles show the neutron entrance channel with a cadmium slit that reduces the beam section to $29 \times 40$ mm$^2$. Numbers refer to the analyzer rings; the innermost ring 1 is taken out of operation because it is contaminated by the direct beam.

## III. SIMULATION

### A. Software

To investigate the effect of geometric imperfection on the resolution of backscattering spectrometers, a dedicated simulation program has been developed. The program, written in the programming language C, is called BASTSCHO (backscattering trajectory simulation from the chopper onwards, or "fair enough" in Bavarian German). It is placed under the GNU General Public License and attached to this publication as a supplementry material.[3] No further work on this code is planned, because it will be merged into a forthcoming more comprehensive program that simulates multiple scattering as well as resolution effects.[4]

As input, BASTSCHO reads a configuration file that specifies the geometry of analyzers and detectors. On output, it generates simulated resolution spectra. The simulated spectra shown in the following are averages over $N = 100\,000$ neutrons; for explorative runs, $N = 10\,000$ is usually sufficient. Simulated trajectories begin in the graphite deflector crystals in the phase-space transform chopper, and continue via monochromator, sample, analyzer into the detector, unless a neutron misses one of these elements or hits an absorber. The initial neutron position and direction is drawn at random. The trajectory is then fully determined up to the sample. The interaction point within the sample and the direction of the scattered neutron are drawn at random, and the remaining trajectory up to the detector is again deterministic. From the trajectories we obtain the off-backscattering angles $\chi_{i,f}$, and thus (2) the geometric wavenumber shift $\delta k^{\text{geo}}_{i,f}$.

The initial resolution shift $\delta k^{\text{res}}_i$ is drawn at random from the Voigt function that characterizes the intrinsic reflectivity of the monochromator crystals (actually, $\delta k^{\text{res}}_i$ is drawn from a Cauchy (Lorentzian) distribution, and the Voigt distribution is emulated by assigning the trajectory an appropriate

weight). On the detector side, $\delta k$ is swept through all the desired histogram channels, $\delta k_f^{res}$ is computed from (7), and the histogram count is incremented by the trajectory weight multiplied by the analyzer reflectivity at $\delta k_f^{res}$, given again by the Voigt function.

### B. Calibration at large scattering angles

To verify and calibrate the simulation, it is first applied to regular large-angle detectors. The calibration consists in adjusting the widths $\sigma$ and $\gamma$ of the Voigt functions used to simulate the intrinsic resolution broadening in monochromator and analyzer. Since the convolution of two Voigt functions $V(k, \sigma, \gamma)$ yields another Voigt function $V(k, \sqrt{2}\sigma, 2\gamma)$, initial parameter values can be obtained from the fit to the measured large-angle resolution (Sec. II B): $\sigma = \sigma_{fit}/\sqrt{2} = 4.16 \times 10^{-5} k_0$, $\gamma = \gamma_{fit}/2 = 6.30 \times 10^{-6} k_0$. Using these values, the simulation reproduces already quite well the experimental resolution spectrum, confirming the estimate from Sec. II C that geometric effects are unimportant in regular backscattering detectors. Nevertheless, the agreement of simulation and experiment can be slightly improved by reducing the Lorentzian width parameter. In the following, we work with $\gamma = 6.0 \times 10^{-6} k_0$. For better comparison with experimental data, simulated data also include a flat background. Figure 2 shows that the simulation agrees with the measured large-angle resolution just as well as the heuristic Voigt fit.

### C. Small-angle resolution reproduced by simulation

We now come to the five small-angle detectors of SPHERES. Figure 4 shows how they are currently arranged around the beam window. Measured and simulated resolution spectra are shown in Fig. 5. As expected from the imperfect geometry, the resolution is broader than in the large-angle detectors, it is much more off-center, and it is asymmetric. Partly as a result of the broadening, the signal-to-noise ratio is much weaker. The resolution cannot be fitted by a Voigt function; nor does its center resemble a Gaussian. Of course, all these are very unfavorable for studying quasielastic scattering.

To match the simulations to the experimental data, we use no more than two adjustable parameters: a detector-dependent background level and an amplitude that is kept fixed for all five small-angle detectors. The amplitude differs from that at large scattering angles, because the detectors are of a different type, and have different discriminator settings. Besides these parameters, the input to the simulation only consists of the intrinsic reflectivity Voigt profile and the instrument geometry. The latter comprises the detector location, the tilt of the analyzer rings, and the location of absorbing elements (the beam stop and the large-angle detector block, which is partly in the way of the outermost analyzer rings).

The simulation reproduces the shift, the height, the width, and the asymmetry of the resolution spectra with good accuracy. This proves that the mediocre resolution of small-angle detectors is mainly due to geometric effects, and it opens new ways to rational improvement by simulation-guided realignment and other modifications of the geometry.

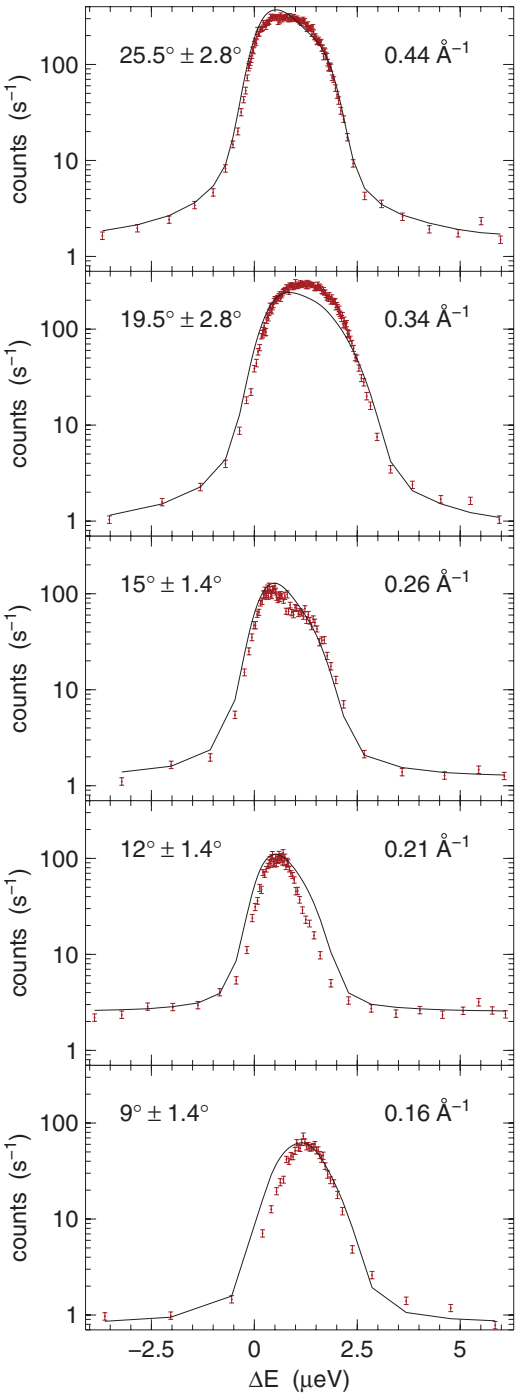


FIG. 5. Resolution spectra of SPHERES at small scattering angles. Standard detector configuration in Fig. 4; analyzers realigned in the course of this study. Sample as in Fig. 2. Solid lines show the corresponding simulations. The only adjusted parameters are overall amplitude, and detector-dependent background level.

Remaining discrepancies between simulation and experiment are mostly due to imperfect knowledge of the actual geometry. This is illustrated in Fig. 6: Assuming that the analyzer center $\boldsymbol{c}$ was about 6 mm away from its nominal position, an almost perfect reproduction of the measured resolution spectrum is achieved. Conversely, a slight extra tilt of the analyzers could be employed on purpose to achieve a narrower resolution. However, it must be ensured that this does not result in neutrons hitting a neighboring detector;

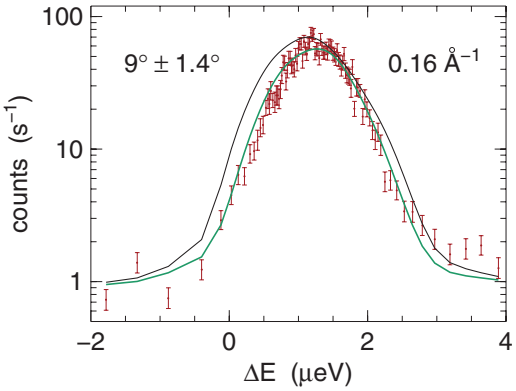


FIG. 6. Resolution spectra of SPHERES at the smallest scattering angle. Same data as in the top frame of Fig. 5 with lesser rebinning. Black line: simulation based on nominal geometry, as in Fig. 5, except for a 12% higher amplitude. Green line: simulation with slightly turned analyzer, focal point at (33, 35, −42) mm instead of (30, 30, −42) mm.

such cross-talk would be an especially undesirable form of background.

## IV. OPTIMIZATION OF SPHERES

### A. Realignment motivated by simulation

The experimental resolution spectra shown in Fig. 5 are the result of simulation-guided realignment. When measurement and simulation were compared for the first time, the agreement was not so good. In particular, there was no way to describe all five small-angle detectors with the same amplitude.

Usually, analyzers are aligned by mechanical or optical means. Deviating from this practice, we readjusted selected degrees of freedom by maximizing neutron counts. This is time-consuming, and without motorization and computer control it is quite laborious, but it proved highly successful for one degree of freedom: Guided by geometric insight, supported by simulation, and confirmed by experiment, we found that the focussing of the outermost analyzer rings depends critically on the distance between the sample and the analyzers. Fortunately, the heavy analyzer assembly is mounted on linear ball-bearing slides with a lead screw drive, so that it can be displaced reproducibly in the relevant direction. A displacement of the order of 1 cm resulted in a 70% gain at $2\theta = 25.5°$.

### B. Partial covering of analyzer rings

As explained in the Introduction, the off-axis location of the small-angle detectors and the corresponding tilt of the analyzer rings break the rotational symmetry around the incident beam and cause the analyzer Bragg angle $2\Theta$ to vary around the ring so that the section opposite the detector is much closer to exact backscattering than the remainder of the ring. The resulting spread of reflection angles contributes to the observed shift, broadening, and asymmetry of the resolution function. We, therefore, got the idea of taking parts of some of the analyzer rings out of operation by covering them with neutron-absorbing cadmium sheets, as shown in Fig. 7.

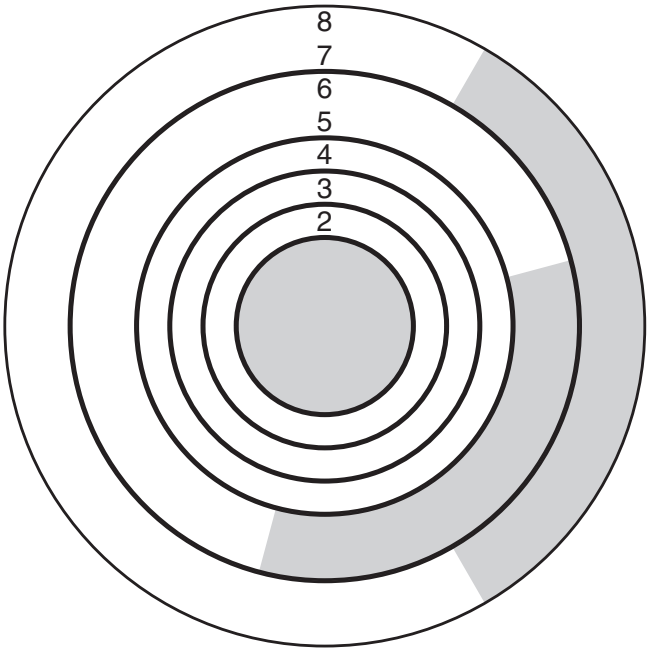


FIG. 7. Small-angle analyzer rings as seen from the chopper. Ring 1 is covered by the central beam stop. The pairs 5/6 and 7/8 are binned into one detector each. Gray-shaded areas indicate the removable Cd sheets that are used to partly cover rings 5–8, leading to an improved resolution as shown in Fig. 5.

Figure 8 shows measured and simulated spectra at $2\Theta = 19.5°$ and 25.5°. For full analyzer rings, the data are the same as in Fig. 5. Additionally, Fig. 8 shows what happens when 120° of the analyzer rings are taken out: The intensity is decreased by about 20% at the peak, but by a factor of 2–3 in the right wing. The experimental realization is in good

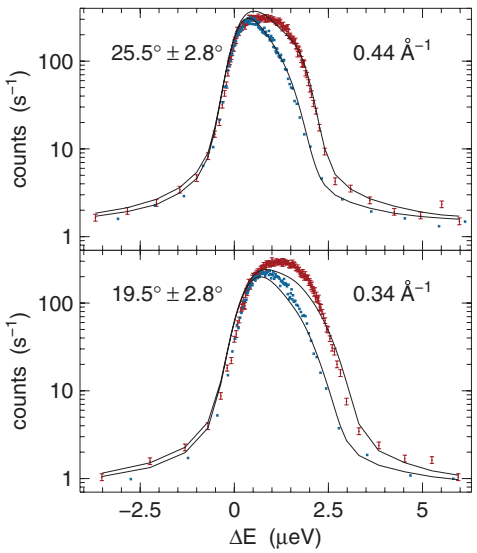


FIG. 8. Resolution spectra of SPHERES in the fourth and fifth of the five small-angle detectors. Red data points and the corresponding simulation are the same as in Fig. 5. The narrower spectra, shown in blue, have been obtained with analyzer rings partly covered with Cd absorber, as explained in Sec. IV B and illustrated in Fig. 7. Solid lines show again the corresponding simulations, with no additional adjusted parameters.

agreement with the simulation. For quasielastic experiments, the reduced shift, width, and asymmetry of the resolution are a huge advantage that clearly outweighs the loss in peak intensity. Therefore, partial cadmium coverage of some large-angle analyzers has now become the standard configuration of SPHERES.

## V. OUTLOOK

Figure 4 shows that the neutron beam window (the exit window of the chopper vacuum housing) is much larger than needed, and much of it is covered by a cadmium diaphragm. In the future, a new, smaller window will allow us to place the detectors closer to the optical axis. This will considerably improve the resolution, since distortions of the resolution function, according to Eq. (10), depend quadratically on the detector displacement.

Figure 4 also shows that the detectors are at some distance from each other. By reducing this distance, the outermost detectors (for rings 2 and 5,6) can be brought closer to the optical axis. However, this should only be done if additional simulations and experiments confirm that it does not lead to perceptible cross-talk.

Finally, a smaller beam window would allow us to place the first regular large-angle counter tube at a scattering angle of only $2\vartheta = 20^\circ$, instead of the present $35^\circ$. However, in order to displace the large-angle analyzer shells towards smaller angles, the outermost small-angle analyzer rings must be removed, which require reengineering of the entire assembly.

Studies of $q$ dependent quasielastic scattering will benefit from these measures.

## ACKNOWLEDGMENTS

We thank Marco Gödel, Hans Kämmerling, Andreas Nebel, Simon Staringer, and Vladmir Ossovyi for technical support.

[1] J. Wuttke, A. Budwig, M. Drochner, H. Kämmerling, F.-J. Kayser, H. Kleines, L. C. Pardo, M. Prager, V. Ossovyi, D. Richter, G. J. Schneider, H. Schneider, and S. Staringer, Rev. Sci. Instrum. **83**, 075109 (2012).
[2] S. G. Johnson and J. Wuttke, see http://apps.jcns.fz-juelich.de/libcerf for *libcerf*, a numeric library providing complex error functions.
[3] See supplementary material at http://dx.doi.org/10.1063/1.4831815 for the source code of the simulation program BASTSCHO.
[4] A. Soininen and J. Wuttke, Thermal Neutron Multiple-Scattering Code msca3. I. Simulating Backscattering Spectroscopy (unpublished); see http://apps.jcns.fz-juelich.de/msca3.